Proc. Natl. Acad. Sci. USA
Vol. 91, pp. 12927–12931, December 1994
Biophysics

Following the assembly of RNA polymerase–DNA complexes in aqueous solutions with the scanning force microscope

MARTIN GUTHOLD*, MAGDALENA BEZANILLA†, DOROTHY A. ERIE*, BETHANY JENKINS*, HELEN G. HANSMA†, AND CARLOS BUSTAMANTE*‡§

*Institute of Molecular Biology and Chemistry Department, ‡Howard Hughes Medical Institute, University of Oregon, Eugene, OR 97403; and †Department of Physics, University of California, Santa Barbara, CA 93106

Communicated by Brian Matthews, September 6, 1994

ABSTRACT **The capability of the scanning force microscope (SFM) to image molecules in aqueous buffers has opened the exciting possibility of following processes of molecular assembly in real time and in near-physiological environments. This capability is demonstrated in this paper by following the assembly process of RNA polymerase–DNA complexes. DNA fragments deposited on mica and imaged in Hepes/$MgCl_2$ are shown *before* and *after Escherichia coli* RNA polymerase holoenzyme is injected in the SFM liquid chamber. The protein can recognize and bind to these DNA fragments within several seconds after injection, suggesting that the protein and the DNA retain their native configuration after deposition and during SFM imaging. A time-lapse sequence depicting the process of assembly of RNA polymerase–DNA complexes is shown. These results represent the first step for acquiring the capabilities to monitor complex biomolecular processes as they take place in ionic solutions and to characterize their spatial organization.**

Rapid growth in the applications of the scanning force microscope (SFM) (1) to biology has occurred in the last 3 years. Images of DNA have been obtained in air (2–8), in propanol (9, 10), in water, and in buffer (10–13). Proteins and protein–DNA complexes (2, 5, 14–25), as well as subcellular structures and whole living cells (26), have been imaged. Moreover, imaging in aqueous solutions has made it possible to visualize supramolecular and cellular processes as they take place. The SFM has been used to study the process of crystal growth of hen lysozyme in solution (27) and to visualize living mammalian cells in changing physiological environments (28).

In this paper the SFM's capability to image molecular processes is demonstrated by following the assembly of nonspecific RNA polymerase–DNA complexes in aqueous solution. The formation of RNA polymerase–DNA complexes was chosen in these studies mainly because (*i*) the large number of binding sites greatly increases the probability of observing the bimolecular reaction within the spatial and temporal limitations imposed by an SFM experiment; (*ii*) both open promoter and elongation RNA polymerase–DNA complexes have been previously imaged in air using SFM (14); (*iii*) the formation of nonspecific complexes is biologically relevant, since it is thought to be the first step in promoter localization by *Escherichia coli* RNA polymerase (29, 30); and (*iv*) the capability to follow these processes will make it possible to characterize the dynamics of such assembly processes and is the first step to use the SFM to elucidate the spatial relationships among factors involved in the control of gene expression.

MATERIALS AND METHODS

Sample Preparation. One to 20 μl of a solution containing 4 mM Hepes, 1 mM $MgCl_2$, and 1 nM DNA fragment (pH 7.4) was deposited onto freshly cleaved ruby mica (Mica New York, New York). A 1258-bp DNA fragment containing the λ P_R promoter, one-fifth from one end, was used in these experiments. After letting the sample set for 10 sec, it was thoroughly rinsed with ≈200 ml of doubly distilled water, using the water beam of a Water Pik or a laboratory squirt bottle. It was then blown dry with a flow of dry nitrogen and put in a vacuum desiccator (over 97% $CaSO_4$/3% $CoCl_2$) for at least 30 min (0.04 Pa) at room temperature. The dehydrated DNA sample was then placed in the liquid cell chamber (Fig. 1) of the SFM and submerged in doubly distilled water. RNA polymerase was purchased from Epicentre Technologies (Madison, WI). To demonstrate the protein's activity, stalled elongation complexes were formed (transcript length, 24 nt; radiolabeled guanine) on the above-mentioned template. The transcript was visualized on a 15% acrylamide/7 mM urea gel (data not shown).

SFM Hardware. All images were obtained with a Nanoscope III (Digital Instruments, Santa Barbara, CA), except images in Fig. 5 *C* and *D*, which were obtained with a Nanoscope II (Digital Instruments). Silicon nitride cantilevers (force constant, K = 0.12 N/m, Digital Instruments) with electron beam-deposited (EBD) tips (31–33) were used. Imaging was done in the liquid cell chamber of the Nanoscope III (Fig. 1). Liquids were exchanged via the connected Teflon hosing and regular 10-ml syringes.

SFM Imaging in Liquids. The liquid cell with the DNA sample was flushed with about 5 ml of doubly distilled water before the initial imaging. After the chamber was filled with water, but prior to imaging, a waiting period ranging from several minutes to 2 hr was required for the microscope to attain mechanical and thermal stability necessary to permit imaging. Subsequently, liquids were exchanged via the hosing and the syringes connected to the liquid chamber. The scanning tip was withdrawn during the liquid exchange. After subsequent liquid exchanges only a short waiting period of ≈2 min was required before scanning could be resumed. In addition to water, imaging was done in four different buffer solutions: (*i*) 10 mM Hepes/1 mM $MgCl_2$, pH 7.4; (*ii*) 10 mM Hepes/10 mM $MgCl_2$/10% glycerol, pH 7.4; and (*iii*) and (*iv*) these buffers containing 1 nM RNA polymerase holoenzyme. The protein was diluted 2000-fold from a stock solution just before it was injected into the liquid cell. The loading force on the sample was typically 3 nN or less.

RESULTS

SFM images of 1258-bp DNA fragments obtained under water are shown in Fig. 2*A*. These images are stable under repeated scans, indicating that the DNA molecules are well

The publication costs of this article were defrayed in part by page charge payment. This article must therefore be hereby marked "*advertisement*" in accordance with 18 U.S.C. §1734 solely to indicate this fact.

Abbreviations: SFM, scanning force microscope (microscopy); EBD tip, electron beam-deposited tip.

§To whom reprint requests should be addressed.

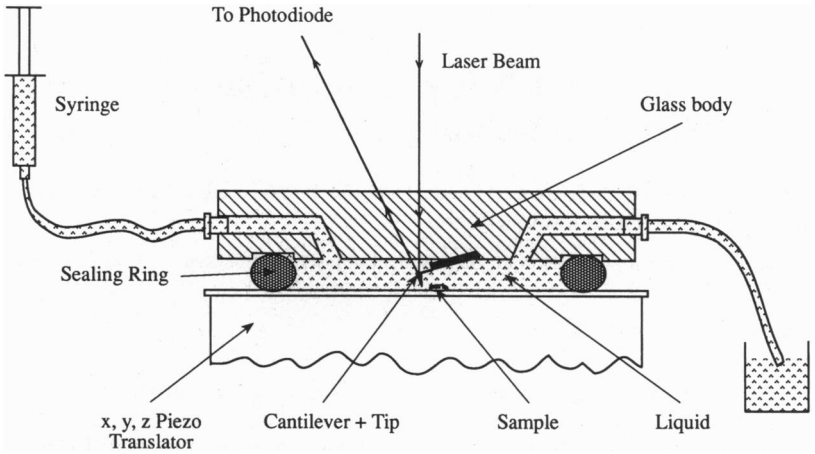

FIG. 1. Cross section of the standard SFM liquid cell in which the RNA polymerase experiments were carried out. It confines a volume of about 30 μl and fluids can be exchanged by carefully flushing them through the cell via the connected hosing and the syringe.

attached to the mica surface. Prior to scanning, the DNA molecules remain stably bound to the surface for several hours. After imaging the DNA in water, the liquid cell is filled with 10 mM Hepes/1 mM $MgCl_2$, pH 7.4, buffer. Similar images were acquired in 10 mM Hepes/10 mM $MgCl_2$/10% glycerol, pH 7.4, buffer solution. Clear and highly resolved images of DNA fragments are obtained also in these ionic solutions (Fig. 2*B*). The average length (±SD) of the DNA fragments is 419 ± 11 nm in water (92 molecules), 416 ± 10 nm in 10 mM Hepes/1 mM $MgCl_2$, pH 7.4, buffer (28 molecules), and 400 ± 24 in 10 mM Hepes/10 mM $MgCl_2$/10% glycerol, pH 7.4, buffer (32 molecules). The DNA molecules in the higher salt buffer are shorter and have a greater standard deviation, presumably because they tend to detach and curl up at the ends during continuous scanning. Nonetheless, in all three environments, the average lengths are within 5% of the expected length for B-DNA (1258 bp × 0.338 nm/bp = 425 nm).

Once stable imaging of the DNA fragment has been established in Hepes/$MgCl_2$ buffer, 300 μl of 1 nM RNA polymerase holoenzyme diluted in the same buffer is injected into the liquid cell. Fig. 3 displays two consecutive 1500 nm × 1500 nm frames obtained within 2 min (Fig. 3*A*) or 3 min, respectively (Fig. 3*B*), after RNA polymerase injection. In both frames, high features about 200 Å in diameter, identified as RNA polymerase molecules[§] (34), can be seen on the mica surface (Fig. 3*B*, short thin arrow) or being dragged by the tip (Fig. 3*A*, short thick arrow). However, most RNA polymerase molecules can be recognized in both frames *before* (Fig. 3*A*) and *after* (Fig. 3*B*) RNA polymerase binding has occurred (long thin arrows). In the course of these experiments, >20 such individual binding events were recorded.

Fig. 4 shows close-up views of two DNA molecules imaged before and after complex assembly. Upon binding (Fig. 4 *B* and *D*), the RNA polymerase molecules appear as distinct high features setting astride the DNA molecules. RNA polymerase binding occurs at different positions along the DNA fragment, indicating that the observed binding is nonspecific.

Further evidence of the interaction between RNA polymerase and the immobilized DNA molecules can be seen in a time-lapse sequence of consecutive images taken during the RNA polymerase binding event (Fig. 5). A free DNA molecule is shown in Fig. 5*A*. Then, during the scanning process, an RNA polymerase molecule approaches the DNA fragment from the left and binds to it (Fig. 5 *B–F*). In Fig. 5*B* as the tip progresses from the top to the bottom of the frame, the RNA

[§]The dimensions of the RNA polymerase are about 160 Å × 100 Å × 100 Å (34). However, the protein dimensions as seen with the SFM are wider due to tip convolution, which adds about twice the tip radius (50–100 Å) to the real width (3).

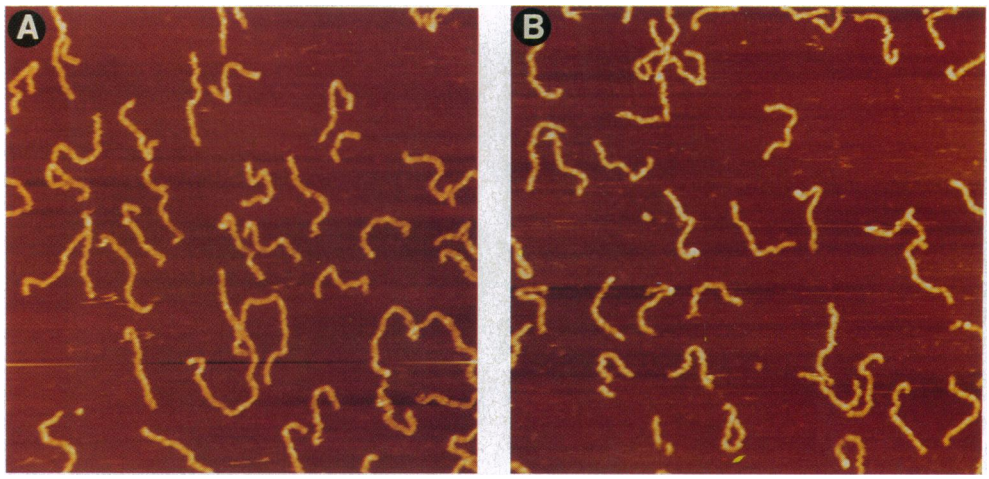

FIG. 2. SFM image of 1258-bp DNA fragments in water (*A*) and 10 mM Hepes/1 mM $MgCl_2$, pH 7.4, buffer (*B*). The image size is 2000 nm × 2000 nm and the horizontal color scale ranges from 0 nm (dark-brown) to 10 nm (white). Both images are flattened and the scan rate is 7.6 scan lines per sec (512 lines per image).

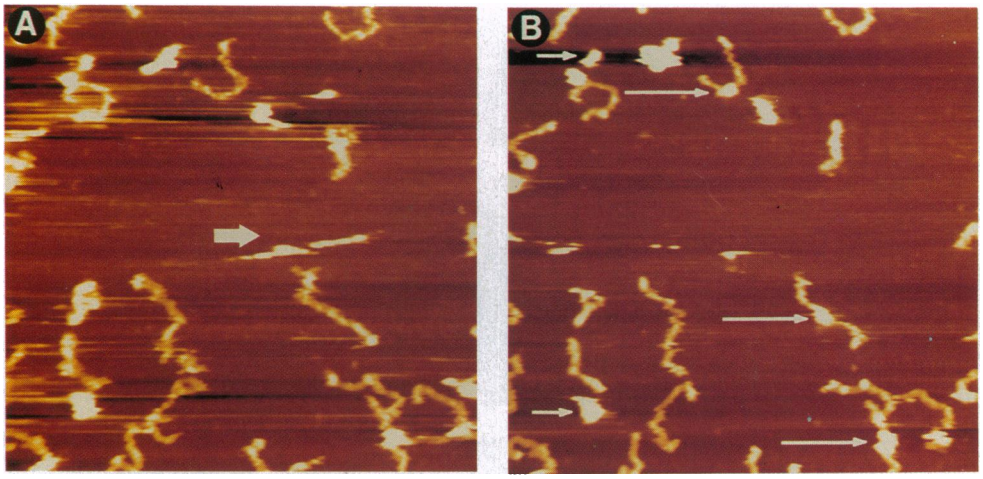

FIG. 3. Two consecutive SFM scans of the DNA sample after flushing the liquid cell with RNA polymerase solution. (*A*) SFM image ≈2 min after RNA polymerase injection (first scan after protein injection). (*B*) SFM image ≈3 min after RNA polymerase injection (second scan after protein injection). Several DNA molecules can be recognized in both frames prior to (*A*) and after binding (*B*) of the RNA polymerase (long thin arrows). RNA polymerase molecules are also binding to the surface (short thin arrows) or being dragged across the surface (short thick arrows). The image size is 1500 nm × 1500 nm and the height scale is the same as in Fig. 2. Both images are flattened and the scan rate is 7.6 scan lines per sec (512 lines per image).

polymerase molecule that is initially on the left side of the DNA (Fig. 5*B*, short arrow) suddenly changes position and binds to the DNA molecule (Fig. 5*B*, long arrow). Presumably, either the RNA polymerase molecule is pushed by the scanning tip or it diffuses on the surface until it binds to a DNA molecule. Once bound, the RNA polymerase molecule

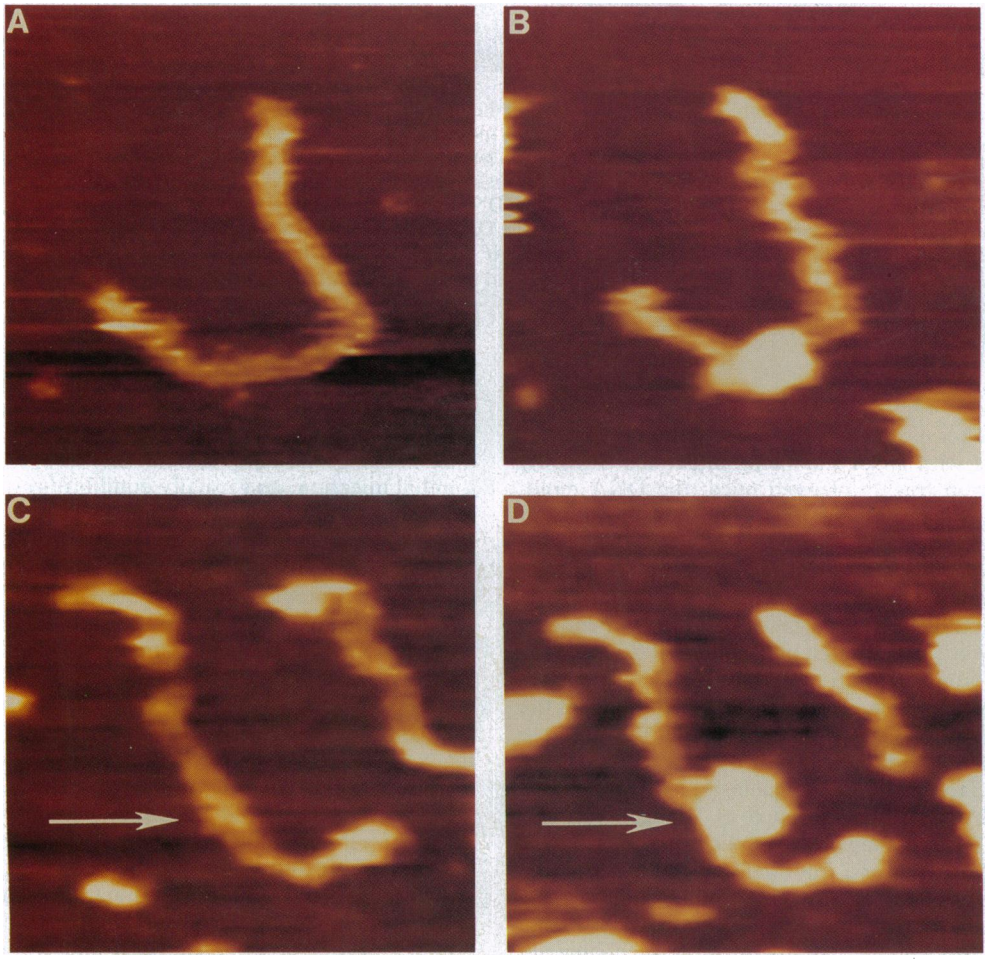

FIG. 4. Close-up views of two DNA molecules before (*A* and *C*) and after (*B* and *D*) binding. Images *A* and *B* are close-up views of two molecules in Fig. 3. Images *C* and *D* were taken in 10 mM Hepes/10 mM $MgCl_2$/10% glycerol, pH 7.4, buffer. In images *C* and *D* the DNA appears to become distorted toward the RNA polymerase upon binding (arrow). The image size is 300 nm × 300 nm and the height scale is the same as in Fig. 2. The images are flattened and the scan rate is 7.6 scan lines per sec (512 lines per image) in images *A* and *B* and 5.0 scan lines per sec (400 lines per image) in images *C* and *D*.

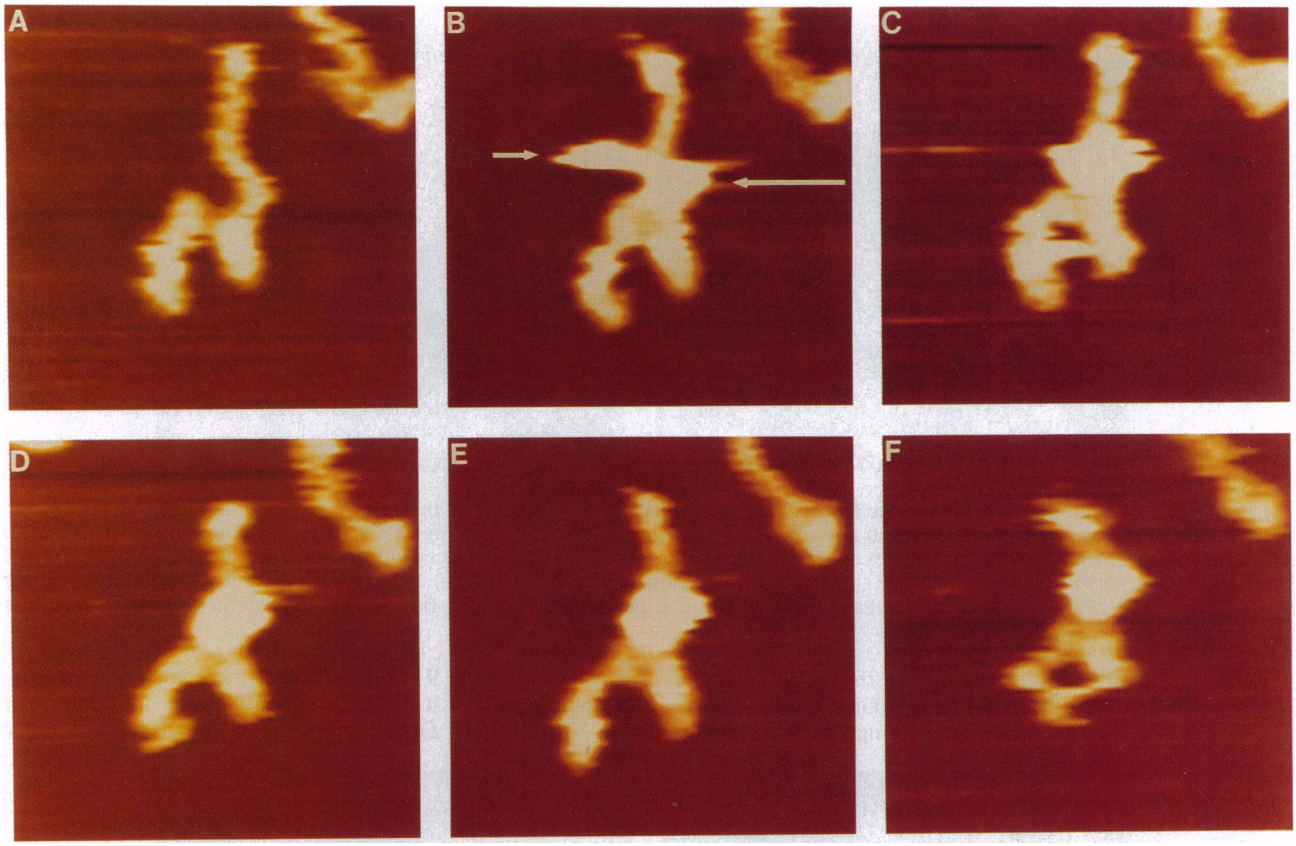

FIG. 5. Time-lapse sequence of consecutive SFM images showing the binding process of RNA polymerase to the DNA template (all images are taken in 10 mM Hepes/1 mM $MgCl_2$, pH 7.4, buffer). (*A*) Free DNA molecule. (*B*) RNA polymerase molecule approaching the DNA fragment followed by binding to the DNA. While the tip is scanning downward, an RNA polymerase molecule is binding to the mica surface just left of the DNA. The top part of the RNA polymerase is therefore seen some distance away from the DNA (short arrow). However, as the tip is scanning on top of the RNA polymerase, the protein suddenly moves toward the DNA molecule (presumably pushed by the tip) and binds to it (long arrow). In subsequent scans (*C–F*) the RNA polymerase is tightly bound to the DNA fragment as it does not detach even under repeated scanning. Only after five consecutive scans does the complex deteriorate somewhat (*F*). Size, scan speed, and filtering in all images are the same as in Fig. 4 *A* and *B*.

remains associated with the DNA and can be scanned repeatedly (Fig. 5 *C–F*).

DISCUSSION

Five factors were required to image reliably the assembly of RNA polymerase with DNA fragments under the SFM. (*i*) Upon deposition on freshly cleaved mica, the DNA molecules must be thoroughly rinsed to wash off loosely attached DNA molecules and salt deposits, leaving only the tightly bound DNA on a clean surface. Approximately 80% of the attached DNA was removed by this rinsing step (13). (*ii*) To stabilize their binding to the surface, the DNA molecules must be subsequently dehydrated in a vacuum desiccator for at least one-half hour at room temperature (12, 23). Dehydration of the DNA appeared to strengthen the binding of the DNA molecules to the mica by excluding water between the molecules and the mica surface and/or by making it possible for the ions associated with the molecules to bind to the mica surface. (*iii*) A hydrophobic tip [such as EBD carbon tips (31–33)] must be used to image hydrophilic molecules. These tips are minimizing adhesive interactions with hydrophilic molecules, thereby reducing mechanical distortions of the sample and preventing removal of the molecules from the surface (12, 23). (*iv*) The microscope must be mechanically stable and free of thermal drift to maintain a minimum loading force acting on the sample. The tip was disturbed most after introducing liquid into the cell for the *first* time, as initial hydrodynamic drag forces and thermal changes led to significant mechanical instabilities. Waiting periods of up to 2 hr were then required for the tip to reach mechanical and thermal equilibrium. In particular, tip noise vertical to the scanning direction made it impossible to obtain images before equilibrium was attained, whereas drift in the horizontal direction often permitted stable imaging. Careful, subsequent exchange of the liquid did not disturb the tip as much as the initial injection, and usually equilibrium was reached within 1–5 min. (*v*) Certain buffers appeared to stabilize the attachment of molecules to the surface during imaging. Hepes, for example, stabilized the binding of DNA to mica, whereas Tris tended to promote detachment of DNA, either by weakening the bonding of the molecules to the surface or by increasing the tip–molecule adhesive interactions (12, 13). Because of the many factors required to obtain high-quality images, only about 20% of the imaging sessions were successful.

The observation that RNA polymerase could bind to the DNA suggests that both molecules retained their native configuration under the conditions of these experiments. This result could not have been predicted *a priori*, since the DNA molecules were attached to the surface and the RNA polymerase must diffuse on the mica surface prior to binding to the DNA. Apparently, protein–DNA interactions, in which electrochemical forces play a major role, can also take place under SFM imaging conditions and while the DNA is attached to a mica surface.

Most of the binding events observed in the course of these studies were nonspecific, which is to be expected given the great excess of nonspecific binding sites over the promoter sites and the ratio of specific and nonspecific binding con-

stant expected at the prevalent solution conditions. The dissociation constants at the ionic conditions used in our experiments are $\approx 10^{-7}$ M and $\approx 10^{-10}$ M, for nonspecific binding (35) and for specific binding to the λ P_R promoter (36), respectively. However, the concentration of nonspecific sites is 1000 times in excess of promoter concentration. It is not possible to estimate at this point how the presence of the charged mica surface may affect the relative value of these two binding constants.

Although RNA polymerase bound mostly nonspecifically to the DNA, one-dimensional diffusion of the RNA polymerase along the DNA molecule was not observed. There might be two reasons for this. First, the DNA molecules, being stably attached to the mica surface, may prevent the spiraling motion that the protein might describe around the DNA if it is to maintain an invariant relationship with the DNA surface (37). Second, even though the RNA polymerase bound to the DNA, it is possible that it still interacted with the mica surface upon DNA binding. Accordingly, ways of controlling externally the strength of attachment of molecules to the substrate, such as would be possible with electro-deposition methods (38), need to be developed. These designs would make it possible to partially detach from the surface a preassembled complex, to facilitate its complexation with an additional component, before the whole assembly is reattached to the substrate.

The results presented here show that the SFM can be used to investigate biological structures in aqueous environments at molecular resolution. These results also indicate the feasibility of using the SFM to follow and monitor molecular processes involved in the recognition and formation of complex macromolecular assembly processes under aqueous solutions. Thus, a whole range of biological structures, whose complexity is presently beyond traditional structural methods, will become accessible to structural characterization in physiologically relevant environments. In particular, investigation of the spatial and molecular relationships involved in the formation of functional assemblies, such as eukaryotic transcription complexes, may soon be possible. To carry out such studies, it may be necessary to preassemble some of the factors on the DNA, prior to deposition on mica, to encourage the specific assembly of additional factors under the liquid cell. Other technical improvements such as the development of sharper tips and the implementation of *noncontact* (39) and *tapping* (40, 41) imaging under liquids will greatly facilitate the study of these systems.

We thank the von Hippel laboratory for help in the preparation of some of the samples and for providing the plasmid with the DNA fragment used in these studies. We thank G. Yang for assistance with the SFM. This work was supported by National Science Foundation (NSF) Grants MBC 9118482 and BIR 9318945 to C.B., National Institutes of Health Grant GM-32543 to C.B., and NSF Grant DIR 9018846 to H.G.H. This work was supported in part by a grant from the Lucille P. Markey Foundation to the Institute of Molecular Biology.

1. Binnig, G., Quate, C. F. & Gerber, C. (1986) *Phys. Rev. Lett.* **56,** 930–933.
2. Bustamante, C., Vesenka, J., Tang, C. L., Rees, W., Guthold, M. & Keller, R. (1992) *Biochemistry* **31,** 22–26.
3. Vesenka, J., Guthold, M., Tang, C. L., Keller, D., Delaine, E. & Bustamante, C. (1992) *Ultramicroscopy* **42–44,** 1243–1249.
4. Zenhauser, F., Adrian, M., Ten Heggler-Bordier, B., Emch, R., Jobin, M., Taborelli, M. & Descouts, P. (1992) *J. Struct. Biol.* **108,** 69–73.
5. Yang, J., Takeyasu, K. & Shao, Z. (1992) *FEBS Lett.* **301,** 173–176.
6. Thundat, T., Warmack, R. J., Alison, D. P., Bottomley, L. A., Lourenco, A. J. & Ferrel, T. L. (1992) *J. Vac. Sci. Technol. A* **10,** 630–635.
7. Henderson, E. (1992) *Nucleic Acids Res.* **20,** 445–447.
8. Samori, B., Siligardi, G., Quagliariello, C., Weisenhorn, A. L., Vesenka, J. & Bustamante, C. J. (1993) *Proc. Natl. Acad. Sci. USA* **90,** 3598–3601.
9. Hansma, H. G., Vesenka, J., Siegerist, C., Kelderman, G., Morret, H., Sinsheimer, R. L., Elings, V., Bustamante, C. & Hansma, P. K. (1992) *Science* **256,** 1180–1184.
10. Lyubchenko, Y. L., Oden, P. I., Lamper, D., Lindsay, S. M. & Dunker, K. A. (1993) *Nucleic Acids Res.* **21,** 1117–1123.
11. Lindsay, S. M., Nagahara, L. A., Thundat, T., Knipping, U., Rill, R. L., Drake, B., Prater, C. B., Weisenhorn, A. L., Gould, S. A. C. & Hansma, P. K. (1989) *J. Biomol. Struct. Dyn.* **7,** 279–287.
12. Hansma, H. G., Bezanilla, M., Zenhauser, F., Adrian, M. & Sinsheimer, R. L. (1993) *Nucleic Acids Res.* **21,** 505–512.
13. Bezanilla, M., Bustamante, C. & Hansma, H. G. (1994) *Scanning Microsc.* **7,** 1145–1148.
14. Rees, W. A., Keller, R. W., Vesenka, J. P., Yang, G. & Bustamante, C. (1992) *Science* **260,** 1646–1649.
15. Yang, J., Tamm, L. K., Tillack, T. W. & Shao, Z. (1993) *J. Mol. Biol.* **229,** 286–290.
16. Edstrom, R. D., Meinke, M. H., Yang, X., Yang, R., Elings, V. & Evans, D. F. (1990) *Biophys. J.* **58,** 1437–1448.
17. Weisenhorn, A. L., Drake, B., Prater, C. B., Gould, S. A. C., Hansma, P. K., Ohnesorge, F., Egger, M., Heyn, S.-P. & Gaub, H. E. (1990) *Biophys. J.* **58,** 1251–1258.
18. Ohnesorge, F., Heckl, W. M., Häberle, W., Pum, D., Sara, M., Schindler, H., Schilcher, K., Kiener, A., Smith, D. P. E., Sleytr, U. B. & Binnig, G. (1992) *Ultramicroscopy* **42–44,** 1236–1242.
19. Mulhern, P. J., Blackford, B. L. & Jericho, M. H. (1992) *Ultramicroscopy* **42–44,** 1214–1221.
20. Drake, B., Prater, C. B., Weisenhorn, A. L., Gould, S. A., Albrecht, T. R., Quate, C. F., Cannell, D. S., Hansma, H. G. & Hansma, P. K. (1989) *Science* **243,** 1586–1589.
21. Hoh, J. H., Lal, R., John, A., Revel, J.-P. & Arnsdorf, M. F. (1991) *Science* **253,** 1405–1408.
22. Engels, A. (1991) *Annu. Rev. Biophys. Biophys. Chem.* **20,** 79–109.
23. Bustamante, C., Keller, D. & Yang, G. (1993) *Curr. Opin. Struct. Biol.* **3,** 363–372.
24. Hansma, H. G. & Hoh, J. H. (1994) *Annu. Rev. Biophys. Biomol. Struct.*, in press.
25. Karrasch, S., Hegerl, R., Hoh, J. H., Baumeister, W. & Engel, A. (1994) *Proc. Natl. Acad. Sci. USA* **91,** 836–839.
26. Hoh, J. H. & Hansma, P. K. (1992) *Trends Cell Biol.* **2,** 208–213.
27. Durbin, S. D., Carlson, W. E. & Saros, M. T. (1993) *J. Phys. B.* **26,** 128–132.
28. Barbee, K., Davies, P. F. & Lal, R. (1994) *Circ. Res.* **74,** 163–171.
29. Rodriguez, R. & Chamberlin, M., eds. (1982) *Promoters: Structure and Function* (Praeger, New York).
30. Berg, O. G. & von Hippel, P. H. (1985) *Annu. Rev. Biophys. Biophys. Chem.* **14,** 131–159.
31. Ichihashi, T. & Matsui, S. (1988) *J. Vac. Sci. Technol. B* **6,** 1869–1872.
32. Akama, Y., Nishimura, E., Sakai, A. & Murakami, H. (1990) *J. Vac. Sci. Technol. A* **8,** 429–433.
33. Keller, D. J. & Chih-Chung, C. (1992) *Surf. Sci.* **268,** 333–339.
34. Darst, S. A., Kubaleck, E. W. & Kornberg, R. D. (1989) *Nature (London)* **340,** 730–732.
35. de Haseth, P. L., Lohman, T. M., Burgess, R. R. & Record, M. T. (1978) *Biochemistry* **17,** 1612–1622.
36. Roe, J. H., Burgess, R. R. & Record, M. T. (1984) *J. Mol. Biol.* **176,** 495–521.
37. Schurr, J. M. (1979) *Biophys. Chem.* **9,** 413–414.
38. Lindsay, S. M., Tao, N. J., DeRose, J. A., Oden, P. I., Lyubchenko, Y. L. & Shlyakhtenko, L. (1992) *Biophys. J.* **61,** 1570–1584.
39. Ohnesorge, F. & Binnig, G. (1993) *Science* **260,** 1451–1456.
40. Hansma, P. K., Cleveland, J. P., Radmacher, M., Walters, D. A., Hiller, P., Bezanilla, M., Fritz, M., Vie, D., Hansma, H. G., Prater, C. B., Massie, J., Fukungaga, L., Gurley, J. & Elings, V. (1994) *Appl. Phys. Lett.* **64,** 1738–1740.
41. Putman, C. A. J., Van der Werft, K. O., De Grooth, B. G., Van Hulst, N. F. & Greve, J. (1994) *Appl. Phys. Lett.* **64,** 2454–2456.